THE ASTROPHYSICAL JOURNAL, 492:767–777, 1998 January 10

DISSECTING CAPELLA'S CORONA: GHRS SPECTRA OF THE Fe XXI λ1354 AND He II λ1640 LINES FROM EACH OF THE CAPELLA STARS[1]

JEFFREY L. LINSKY AND BRIAN E. WOOD[2]
JILA, University of Colorado, and National Institute of Standards and Technology, Boulder, CO 80309-0440;
jlinsky@jila.colorado.edu, wood@cfa240.harvard.edu

AND

ALEXANDER BROWN AND RACHEL A. OSTEN
Center for Astrophysics and Space Astonomy (CASA), University of Colorado, Boulder, CO 80309-0389;
ab@echidna.colorado.edu, raosten@mensae.colorado.edu
Received 1997 July 3; accepted 1997 August 21

ABSTRACT

We report on moderate ($\lambda/\Delta\lambda = 20{,}000$) and high ($\lambda/\Delta\lambda = 90{,}000$) resolution spectra of the 104-day period Capella binary system (HD 34029) obtained with *Hubble Space Telescope's* Goddard High-Resolution Spectrometer (GHRS) on 1995 September 9 and 1996 April 9. The observations include a long-duration, moderate-resolution spectrum of the coronal Fe XXI λ1354 line and both moderate- and high-resolution spectra of the He II λ1640 multiplet.

Our objective in observing the Fe XXI line formed at $T = 1 \times 10^7$ K is to determine for the first time the line shape parameters and the contribution of each star's corona. This is feasible because the GHRS can resolve the 53 km s^{-1} radial velocity separation of the stars. Our analysis led to four surprising results: (1) The contribution of the slowly rotating G8 III star to the total Fe XXI λ1354 flux is similar to that of the more active rapidly rotating G1 III star, in contrast to other UV lines formed at lower temperatures. (2) The centroid velocities of the Fe XXI lines from both stars are near their respective photospheric radial velocities. Thus, there is no evidence for downflows or winds, and the hot coronal plasma must be confined, presumably by strong, closed magnetic fields. This is the first direct kinematic evidence for magnetic confinement in the corona of a giant star. (3) The line widths are thermal, indicating very low turbulence ($\xi < 23$ km s^{-1}) compared with the 54 km s^{-1} thermal speed. (4) Our analysis of *Extreme-Ultraviolet Explorer* (*EUVE*) spectra that include four Fe XXI lines shows that the volume emission measures of these lines are about a factor of 3 smaller than for the λ1354 line, which was observed several months after the closest *EUVE* observation. We consider possible explanations for this discrepancy and conclude that variability of the high-temperature coronal emission is the most likely explanation.

We observed the He II λ1640 line twice with a time separation of 7 months, corresponding to about 2 orbital periods. The profiles are nearly identical, except for a large difference in flux near the expected radial velocity of the G8 III star. We believe that the broad He II emission produced by the G1 star is formed mostly by collisional excitation in its transition region, while the emission from the G8 star is produced predominantly by a photoionization/recombination process driven by EUV radiation from the G8 star's corona. The He II λ1640 flux that we measure from the G8 star is consistent with predictions based on *EUVE* flux measurements. The decrease in the λ1640 emission from the G8 star between the phase 0.73 and 0.78 measurements indicates that its EUV radiation is variable, as is observed by *EUVE*.

Subject heading: binaries: spectroscopic — stars: chromospheres — stars: coronae — stars: individual (Capella, α Aurigae) — ultraviolet: stars

1. INTRODUCTION

While the *ROSAT* and *ASCA* are providing important information on the X-ray emission from stellar coronae, these instruments, and even those now under development (e.g., *AXAF* and *XMM*), lack the spectral or spatial resolution necessary to separate the X-ray flux from the individual stars in spectroscopic binary systems, or to measure line profile widths or radial velocities. Fortunately, one coronal emission line present in high-resolution ultraviolet spectra of bright, late-type stars can provide for the first time answers to these important questions. This is the Fe XXI λ1354 line, which is detectable with the moderate spectral resolution gratings of the Goddard High-Resolution Spectrograph (GHRS) on board the *Hubble Space Telescope* (*HST*).

Analysis of the Fe XXI line profiles of spectroscopic binary systems can provide emission measures of the 1×10^7 K plasma in the corona of each star when the system is observed at quadrature (maximum radial velocity separation). High-resolution spectra of the Fe XXI λ1354 line can also identify coronal flow speeds and turbulent velocities if present. Such data can determine whether or not coronal ions participate in the wind outflow for active stars with low-β plasmas ($\beta = 8\pi P_{\rm gas}/B^2$). Alternatively, the coronal lines may show redshifts indicative of downflows, as is typically observed for transition region lines. Measurement of line widths can determine whether coronal turbulent velocities are subsonic or supersonic. We can also ask whether the coronal emission measures for 1×10^7 K

[1] Based on observations with the NASA/ESA *Hubble Space Telescope*, obtained at the Space Telescope Science Institute, which is operated by the Association of Universities for Research in Astronomy, Inc., under NASA contract NAS5-26555.

[2] Present address: Harvard-Smithsonian Center for Astrophysics, 60 Garden Street, Cambridge, MA 02138.

plasma inferred from the Fe XXI λ1354 line are consistent with the emission measures inferred from X-ray and EUV spectra. Another important question is which types of stars show He II λ1640 lines formed by collision excitation in the 1×10^5 K transition region plasma, and which types of stars show He II lines formed by recombination and cascade following photoionization of He^+ by X-ray and EUV radiation?

The Capella binary system, consisting of a G1 III star and a G8 III star with a 104-day orbital period, is an ideal target for answering these questions, because Capella is the brightest UV and X-ray source among the late-type spectroscopic binary systems, and because the radial velocity separation of the two stars at quadrature is 53 km s^{-1}. Thus, the lines of both stars can be separated with the 15 km s^{-1} resolution of the moderate-resolution GHRS gratings, although modeling will be needed to separate broad lines. The Fe XXI line was previously observed in moderate-dispersion GHRS spectra of the dM0e star AU Mic (Maran et al. 1994) and the RS CVn–type binary system HR 1099 (Robinson et al. 1996).

2. GHRS OBSERVATIONS OF CAPELLA

We observed Capella (HD 34029) on 1995 September 9 and on 1996 April 9 using the moderate-resolution G140M and G160M gratings and the high-resolution Ech-A grating of the GHRS. For a description of the GHRS instrument, see Brandt et al. (1994), Heap et al. (1995), and Soderblom et al. (1994). Table 1 summarizes the observations, including the spectral ranges and resolutions and integration times. The echelle data were obtained with the small science aperture (SSA) in the FP-SPLIT mode to reduce fixed-pattern noise. The moderate-resolution spectra were obtained through the large science aperture (LSA) to obtain accurate fluxes. All of the data were processed with the CALHRS software (Soderblom et al. 1994). Images of the platinum calibration lamp were taken prior to all observations and used for wavelength calibration.

In this paper, we focus on the observations of the Fe XXI λ1354 and He II λ1640 lines. An analysis of interstellar absorption features present in the C II λλ1335, 1336 lines has already been performed by Wood & Linsky (1997). Analysis of other important spectral features in this data set will be presented elsewhere.

Figure 1 shows the moderate-resolution G160M spectrum of the 1343–1380 Å region with identifications of the Fe XXI line and lines of C I, O I], Cl I, Fe II, and O V. Most of these lines were seen in the AU Mic and HR 1099 spectra of Maran et al. (1994) and Robinson et al. (1996), and all of them are observed in the solar spectrum (Sandlin et al. 1986). The two features marked with a question mark in Figure 1 are unidentified lines seen in the solar spectrum.

3. ANALYSIS OF THE Fe XXI SPECTRAL REGION

3.1. *Chromospheric and Transition Region Lines*

In previous studies, attempts to separate the contributions of the G1 and G8 stars from the blended UV line profiles of the Capella system used both multi-Gaussian–fitting techniques and analyses of line centroid variations with orbital phase (Wood & Ayres 1995; Linsky et al. 1995; Ayres 1984, 1988). These line separation techniques are complicated by the large intrinsic widths of most of the lines, which results in a highly blended profile. Fortunately, most of the lines shown in Figure 1 are relatively weak chromospheric lines, which are much narrower than the transition region and strong chromospheric lines that have been analyzed previously. (The Fe XXI and O V lines are exceptions.) Therefore, we can separate the contribution of each star to an extent not possible before in any other Capella spectrum.

Figure 2 displays many of the individual lines in the Fe XXI spectral region. Almost all of them show a double-peaked shape, showing very clearly the presence of emission from both stars. Despite their small fluxes, these lines were observed with remarkably high signal-to-noise ratio (S/N ≈ 90 at the tops of the O I] lines) thanks to the long exposure time used to detect Fe XXI. Thus, we can easily measure the G1 and G8 star components of each spectral line using two-Gaussian fits. The fits to the relatively unblended lines are shown in Figure 2, and the fit parameters for all of the lines in this spectral region are given in Table 2. This table lists the line identifications, the measured wavelengths, line velocities relative to the photospheric radial velocities, line fluxes, widths, and the reduced χ_ν^2 values for the Gaussian fits. The χ_ν^2 values for the fits to the O I] and Cl I lines are very high, and there are noticeable systematic discrepancies between the fits and the data. These discrepancies could be due to small blends in the profile, uncertainties in the shape of the underlying contin-

TABLE 1

SUMMARY OF GHRS OBSERVATIONS OF CAPELLA

Grating	Aperture and Substep Pattern	Spectral Range (Å)	Spectral Resolution (km s^{-1})	Exposure Time (s)	Start Time (UT)	Important Features
1995 September 9 (Phase 0.73)						
G160M.....	LSA 5	1462–1498	16.2	1777	21:02	N IV]
	LSA 5	1636–1672	14.0	1077	22:21	He II, O III]
	LSA 5	1343–1380	17.6	9694	22:44	Fe XXI, C I, O I]
1996 April 9 (Phase 0.78)						
G140M.....	LSA 5	1393–1418	12.0	4084	19:15	Si IV, O IV], S IV]
EA-42	SSA 9	1331–1338	3.6	754	22:40	C II
EA-34	SSA 9	1636–1644	3.5	3288	23:59	He II
1991 April 15 (Phase 0.26)						
G160M.....	LSA 8	1637–1672	20.0	108	05:46	He II

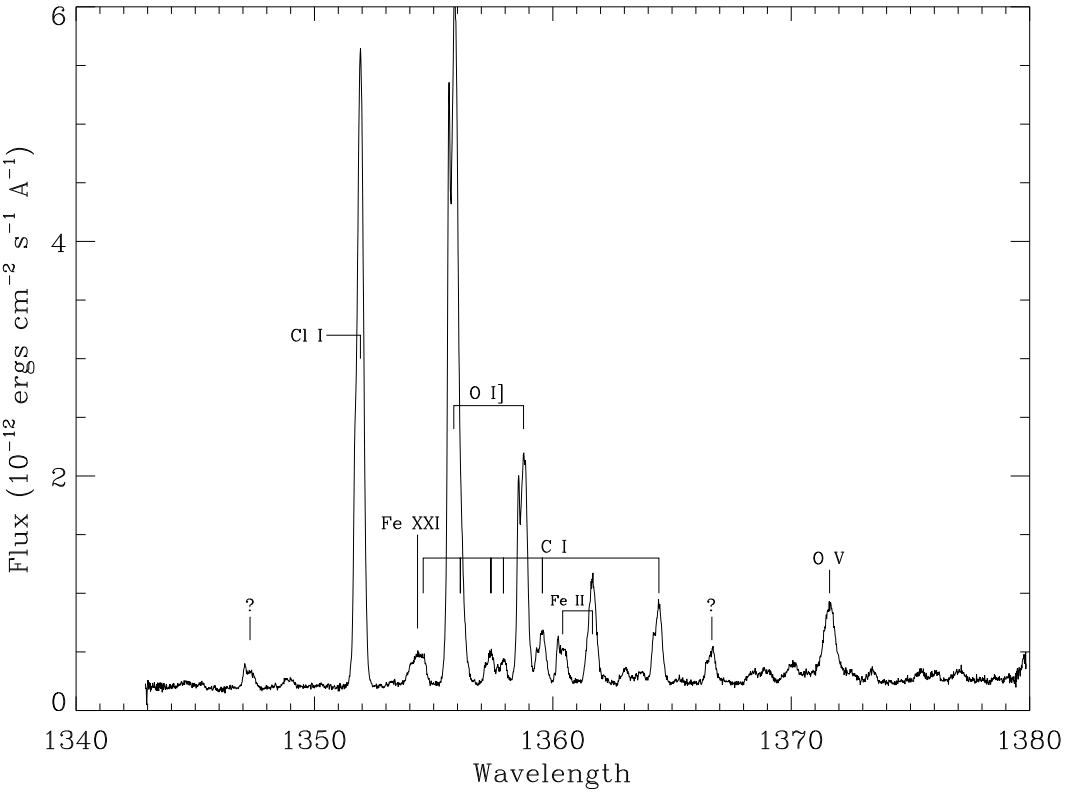

FIG. 1.—G160M medium-resolution spectrum of the 1343–1380 Å spectral region showing Fe XXI and other spectral lines. Note that the Fe XXI feature is blended with a C I line.

uum, or an intrinsic non-Gaussian behavior in these emission lines. We note that Carpenter et al. (1991) observed non-Gaussian line shapes in their very high S/N spectra of the C II] lines of α Tau (K5 III). If the Capella line profiles are indeed non-Gaussian, then the nonthermal velocity properties would likely be more complex than the isotropic, homogeneous model implied by the single-Gaussian fits (one per star).

We have corrected for instrumental broadening in all of our fits, using a Gaussian with a width of 4.4 pixels (Gilliland 1994). Following Wood et al. (1996), we also corrected for rotational broadening of the G1 star, assuming a projected rotational velocity of $v \sin i = 36$ km s^{-1}. A similar correction was unnecessary for the G8 star, since $v \sin i$ is only 3 km s^{-1} (Strassmeier & Fekel 1990). Inspection of Figure 2 reveals that the rotational broadening correction results in a significant reduction in the width of the G1 components (*thin solid lines*). Only after the inclusion of rotational broadening do these components broaden and shorten enough to fit the data.

We were gratified to find that the velocities of all of the chromospheric lines lie close to the stellar radial velocity for both the G1 and G8 star components (see Table 2), as expected, with typical small redshifts of 2–4 km s^{-1}. For the G1 star, Linsky et al. (1995) measured somewhat larger redshifts in Capella's Mg II λ2800 and O I λ1300 multiplet lines, which are much brighter and more optically thick chromospheric lines than those listed in Table 2. The G1 star's transition region lines typically have much larger redshifts of 15–25 km s^{-1}.

As expected, the G1 star accounts for most of the flux in all of the lines, except Fe XXI (see below). However, it is surprising how different the flux contributions are for the two Fe II lines. The G8 star accounts for about 16% of the Fe II λ1360.2 line flux, but only about 3% of the Fe II λ1361.4 flux.

There is only one transition region emission line in this spectral region: the O V λ1371 line. This line has several interesting properties. First, it is the only line showing no evidence of any emission from the G8 star. We therefore fitted it with only a single Gaussian. The O V line is broader than the other lines listed in Table 2, which could help to hide the G8 component. Although previous work (e.g., Linsky et al. 1995; Wood & Ayres 1995) had demonstrated that the G8 star typically accounts for only about 10% of Capella's transition region emission, we expected to see some evidence of the G8 star's presence in the line considering the excellent S/N of the data.

The narrower width of the O V line compared with most of Capella's transition region lines is also interesting. We have no explanation for why the O V λ1371 line width (107 km s^{-1}) is so much smaller than the width of the O V] λ1218 line (150 km s^{-1}) measured by Linsky et al. (1995). Both lines should be formed near log $T = 5.4$, and both should be optically thin.

Finally, we are surprised at how well a single Gaussian fits the O V line. Linsky et al. (1995) found that Capella's transition region lines generally have broad wings and cannot be fitted well at all with a single Gaussian, but the fit to the O V line in Figure 2 shows no excess flux in the line wings that would indicate a "broad component" like that used by Linsky et al. (1995) to fit the wings of Capella's other strong transition region lines. We note, however, that the O V line appears to lie on a "plateau" of blended emis-

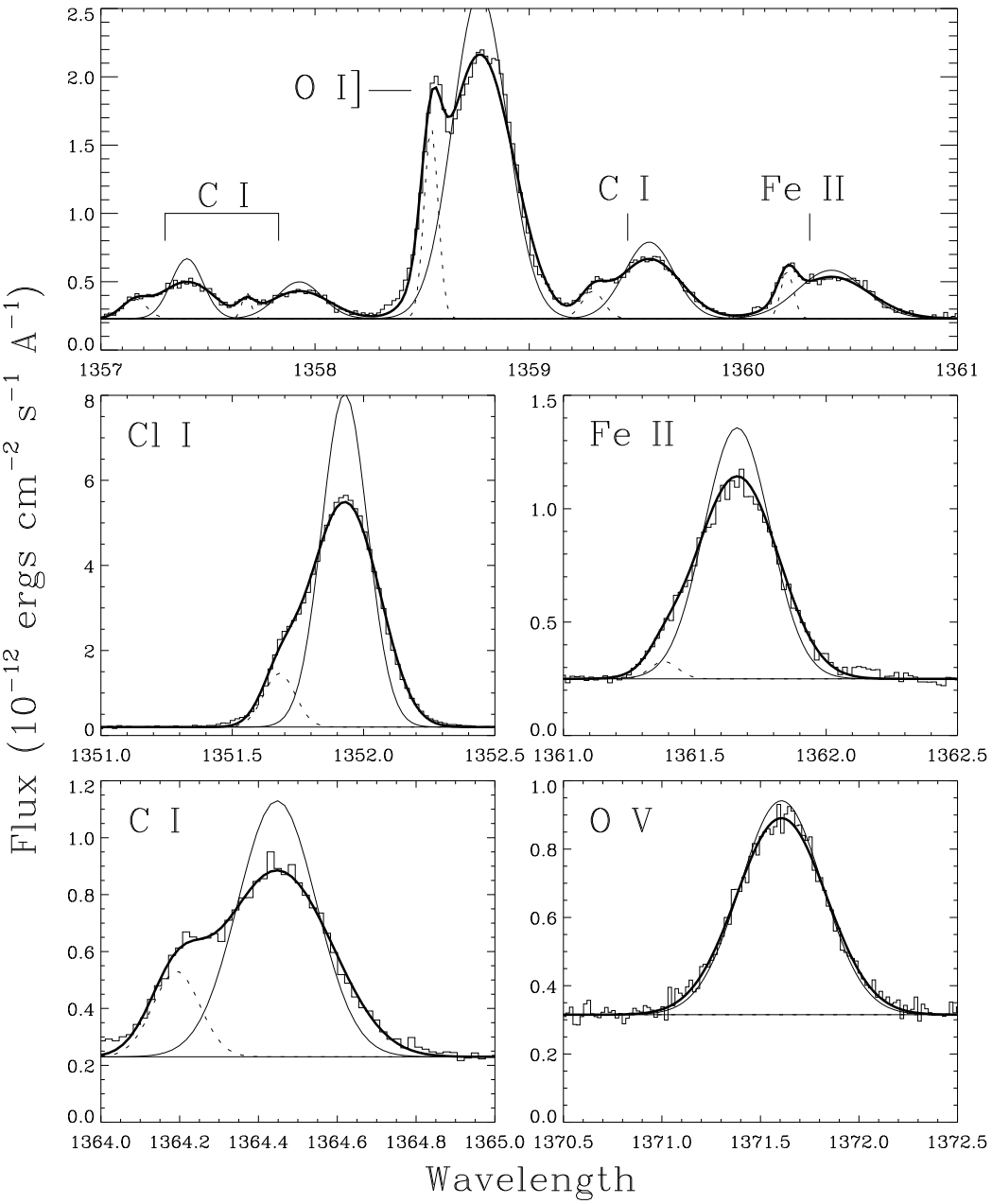

FIG. 2.—Two Gaussian fits to the observed line profiles representing emission from the G1 star (*thin solid lines*), the G8 star (*dotted lines*), and the sum convolved with the instrumental and rotational broadening profiles (*thick solid lines*). The parameters are given in Table 2.

sion lines (see Fig. 1). In Figure 2, we have drawn our continuum line at the top of this plateau, but it is possible that the O V line really does have extended wings that are contributing to the flux of this plateau. If this is the case, then we have underestimated both the line flux and the overall line width, which could also help explain the apparent narrowness of the line relative to Capella's other transition region lines.

3.2. *Analysis of the* Fe XXI λ1354 *Line*

There are two blended features in Figure 1 that required a more complex analysis than that described above for the fits in Figure 2. One contains the O I] λ1356 line, and the other contains the Fe XXI λ1354 line in which we are particularly interested. Both the O I] and Fe XXI lines are blended with C I lines that cannot be separated easily. Fortunately, there are four other C I lines in this spectral region that can be measured easily and used to constrain the properties of the blended C I lines (see Figs. 1 and 2). The average FWHM of the four C I lines is 51 ± 9 and 24 ± 9 km s^{-1} for the G1 and G8 star emission, respectively, where the quoted uncertainties are 1 σ standard deviations. The average C I velocities are 4 ± 2 and 2 ± 1 km s^{-1}.

Figure 3*a* shows our four-Gaussian fit to the Fe XXI + C I blend. The longest wavelength, thin solid line centered at 1354.562 Å is the C I line from the G1 star, and the narrow dotted line centered at 1353.313 Å is the C I line from the G8 star. To simplify the analysis, we have assumed that each component of the C I λ1353 line has the mean FWHM and central velocity measured for the four unblended C I lines. We have also assumed that the line flux ratio (G1/G8) is the same as the mean ratio for the other four C I lines

TABLE 2

LINE PROFILE PARAMETERS[a]

Ion	λ_{rest} (Å)	Star	λ_{meas} (Å)	v[b] (km s^{-1})	f (10^{-14})	FWHM (km s^{-1})	χ^2_ν
?	...	G1	1347.298	...	6.5 ± 0.4	82 ± 6	0.757
		G8	1347.066	...	1.9 ± 0.3	24 ± 4	0.757
Cl I	1351.657	G1	1351.928	3 ± 1	171 ± 1	45 ± 1	7.570
		G8	1351.680	2 ± 1	18.9 ± 0.8	31 ± 1	7.570
Fe XXI	1354.08	G1	1354.324	-3 ± 11	4.8 ± 1.7	87 ± 11	0.915
		G8	1354.084	-3 ± 11	5.9 ± 1.9	87 ± 11	0.915
C I	1354.288	G1	1354.562	(4 ± 2)	6.3 ± 0.7	(51 ± 9)	0.915
		G8	1354.313	(2 ± 1)	1.1 ± 0.3	(24 ± 9)	0.915
O I]	1355.598	G1	1355.845	-2 ± 1	215 ± 4	70 ± 1	17.987
		G8	1355.628	3 ± 1	30.4 ± 0.7	15 ± 1	17.987
C I	1355.844	G1	1356.119	(4 ± 2)	31.2 ± 3.1	(51 ± 9)	17.987
		G8	1355.869	(2 ± 1)	5.6 ± 1.6	(24 ± 9)	17.987
C I	1357.134	G1	1357.402	2 ± 1	8.2 ± 0.4	39 ± 7	1.270
		G8	1357.158	2 ± 2	2.0 ± 0.3	29 ± 4	1.270
C I	1357.659	G1	1357.927	2 ± 1	7.1 ± 0.2	54 ± 3	1.270
		G8	1357.680	1 ± 1	1.0 ± 0.2	11 ± 3	1.270
O I]	1358.512	G1	1358.770	0 ± 1	75.9 ± 0.6	66 ± 1	4.951
		G8	1358.542	3 ± 1	11.4 ± 0.4	17 ± 1	4.951
C I	1359.275	G1	1359.561	6 ± 1	16.2 ± 0.4	60 ± 3	4.951
		G8	1359.298	1 ± 1	2.6 ± 0.4	26 ± 3	4.951
Fe II	1360.17	G1	1360.411	-4 ± 1	13.8 ± 0.4	81 ± 3	1.588
		G8	1360.205	4 ± 1	2.6 ± 0.3	15 ± 3	1.588
Fe II	1361.373	G1	1361.661	7 ± 1	33.5 ± 0.4	65 ± 1	1.318
		G8	1361.382	-2 ± 3	1.0 ± 0.3	27 ± 7	1.318
C I	1364.164	G1	1364.447	5 ± 1	22.4 ± 0.5	51 ± 2	1.206
		G8	1364.192	3 ± 1	4.5 ± 0.4	31 ± 2	1.206
?	...	G1	1366.671	...	10.8 ± 0.3	64 ± 3	1.432
		G8	1366.429	...	1.1 ± 0.2	17 ± 5	1.432
O V	1371.292	G1	1371.607	12 ± 1	32.8 ± 0.3	107 ± 1	1.189

[a] Values in parentheses are assumed rather than derived.

[b] The line velocity relative to the star responsible for the emission, assuming stellar photospheric radial velocities of 56.8 and 3.6 km s^{-1} for the G1 and G8 stars, respectively.

($f_{G1}/f_{G8} = 5.6 \pm 1.1$). Thus, in our fitting procedure, only the total flux of the C I lines was allowed to vary. The remaining two broad Gaussians represent the Fe XXI emission from the two stars (the thin line for the G1 star and the dotted line for the G8 star). In order to sufficiently constrain our fit, we forced the widths of the two Fe XXI components to be the same, and we forced their velocities to be the same (with respect to the photospheric radial velocities of their respective stars), but the fluxes of *both* Fe XXI components were allowed to vary. The sum of the four Gaussians convolved with the instrumental and rotational broadening profiles (*thick solid line*) is an excellent fit to the data ($\chi^2_\nu = 0.915$). A similar procedure was performed in separating the O I] λ1355.6 and C I λ1355.8 lines (see Fig. 3*b*), except that we did not find it necessary to constrain the O I] line parameters as we did for Fe XXI. The parameters of both fits are listed in Table 2.

Our analysis of the Fe XXI feature provided several surprising results. First, the line widths (FWHM = 87 ± 11 km s^{-1}) are *not* larger than the expected thermal broadening in a 1×10^7 K coronal plasma, the temperature at which Fe XXI is most abundant (e.g., Arnaud & Raymond 1992). Since the expected thermal broadening at this temperature is FWHM = 90 km s^{-1}, the nonthermal broadening is very small ($\xi < 23$ km s^{-1}) and definitely subsonic. By contrast, large turbulent velocities are typically inferred for the photospheres and chromospheres of giant stars. Turbulent velocity upper limits much smaller than the thermal width of Fe XXI were previously noted for AU Mic (Maran et al. 1994) and for HR 1099 (Robinson et al. 1996). Thus, the Fe XXI line widths for both Capella stars, AU Mic, and HR 1099 provide no kinematic evidence for shock wave heating of the 1×10^7 K plasmas located in their coronae.

Second, the Fe XXI flux from the G8 star is roughly the same as that from the G1 star. This is very different from what is typically seen in Capella's chromospheric lines, where the G1 star is 2–6 times brighter than the G8 star, and in transition region lines, where the G1 star is generally about 10 times brighter. Why are the coronal fluxes nearly equal when the rapidly rotating ($v \sin i = 36$ km s^{-1}) G1 star is known to be very much more active than the slowly rotating ($v \sin i = 3$ km s^{-1}) G8 star? Ayres, Schiffer, & Linsky (1983) predicted that the X-ray fluxes from the two components of the Capella system should be about equal. Their prediction was based on the assumption that Capella's G8 star has similar X-ray emission properties to β Cet (G9.5 III) and μ Vel (G5 III), stars that are known to have transition region emission line fluxes comparable to Capella's G8 star, as well as having similar spectral types. If the G8 star is indeed similar to β Cet and μ Vel, then it should account for about half of Capella's observed X-ray flux. Our Fe XXI spectrum provides the first critical test of this prediction, and our results are consistent with the prediction. Ayres et al. (1983) suggested that the very different behavior of the X-ray and C IV emission from the Capella stars could be due to the transition region emission being most sensitive to the magnetic field structure and thus the rotation rate, whereas the coronal emission is most sensitive to the convective zone depth and thus the spectral type. The HR 1099 binary may represent another example of this unexpected behavior in the relative f_x values of the two members of the system; Robinson et al. (1996) found that

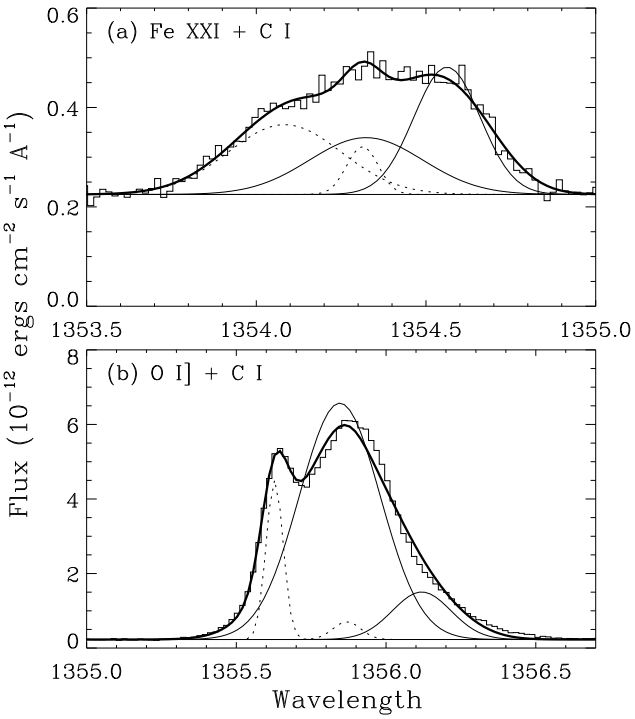

FIG. 3.—(*a*) Four-Gaussian fit to the Fe XXI + C I blend. C I emission from the G8 and G1 stars. The solid (dotted) lines are the G1 (G8) star's Fe XXI and C I lines, where the Fe XXI emission is to the left. The thick solid line is the sum of the four Gaussians convolved with the instrumental and rotational broadening profiles. (*b*) Four-Gaussian fit to the O I] + C I blend. Analogous to (*a*), the solid (dotted) lines are the G1 (G8) star's O I] and C I lines, with the O I] line to the left.

the more slowly rotating G5 IV star contributes about 22% of the total Fe XXI flux from the system, whereas Wood et al. (1996) found that the G5 IV star contributes only 7.5% of the Mg II flux and less than 5% of the transition region line flux.

The line centroid velocities of Fe XXI are difficult to estimate because the rest wavelength is uncertain. In the absence of any laboratory data, Sandlin, Brueckner, & Tousey (1977) adopted 1354.08 $\pm$ 0.05 Å as the rest wavelength using solar flare spectra. We adopt their rest wavelength and find that the centroid velocities of the Fe XXI line for both stars are -3 ± 11 km s^{-1}. We have increased the estimated velocity error because of the lack of laboratory data, but even so the 1×10^7 K plasma in the coronae of both stars is essentially at rest, as was previously found for AU Mic and HR 1099. There are no large downflows (as is seen in many of Capella's transition region lines), and even more surprising, there is no evidence for coronal outflow! Thus, the 1×10^7 K coronal plasma is confined, presumably by closed magnetic field structures. Although confinement of the high-temperature coronal plasma in Capella has been argued previously on the basis of high densities (Dupree et al. 1993), the Fe XXI velocities measured with the GHRS provide the first direct kinematic evidence for confined plasma in the corona of a giant star.

3.3. *Comparison with Other Coronal Emission Lines*

We now compare the Fe XXI λ1354 emission with other coronal emission lines observed by the *Extreme-Ultraviolet Explorer* (*EUVE*) satellite. The *EUVE* spectrum of Capella was described by Dupree et al. (1993), who found that the 80–400 Å spectrum is dominated by coronal emission lines of Fe XV–XXIV. Several Fe XXI emission lines are present in the *EUVE* short-wavelength (SW) spectrometer range. Capella has been observed by *EUVE* each year from 1992 to 1995 and is being observed on a regular basis. The *EUVE* SW and medium-wavelength (MW) photon data were reduced using tasks in the standard EUV package in IRAF. The SW and MW spectra were then extracted using an optimal extraction routine described more fully by Gagné et al. (1997) and adapted from Lenz & Ayres (1992). The SW and MW spectra were then fitted with a thermal bremsstrahlung continuum with multiple Gaussian lines.

The measured line fluxes are given in Table 3 with the two segments of data from 1994 listed separately to probe short-term variability. For the bright Fe XXI and Fe XIX lines observed in 1992 December, the line fluxes measured in this way lie within 10% of the values obtained by Dupree et al. (1993), but the fluxes of the fainter lines differ considerably, indicating that an accurate treatment of the noise is critical in extracting reliable fluxes for the weak lines. The strongest Fe XXI line is at 128.73 Å, with other lines at 97.88, 102.22, 117.51, and 142.20 Å. However, the λ117.51 line is too strongly blended with Fe XXII λ117.17 to be useful. The λ142.20 line is only detected in the 1992 data set. At other times this line has a 3 σ upper limit of (6–7) $\times 10^{-14}$ ergs cm^{-2} s^{-1}. Table 3 also lists the fluxes for the strong Fe XIX λ108.37 and Fe XVIII λ93.92 lines. Most of the *EUVE* lines are observed to vary by about a factor of 2; only the weak λ97.88 is statistically constant.

The observed line fluxes were corrected for interstellar (IS) absorption using a hydrogen column of 1.8×10^{18} cm^{-2} (Linsky et al. 1993). The IS transmission, T_{IS}, is provided for each line in Table 3. The atomic compilation of Brickhouse, Raymond, & Smith (1995) and the CHIANTI database and routines (Dere et al. 1996) were used to estimate the coronal electron densities and volume emission measures (VEM) implied by these emission lines. The ratio of the λ102.22 and λ128.73 line fluxes appears to be the most reliable density diagnostic and gives values of a few 10^{12} cm^{-3} at all four epochs. The λ97.88/λ128.73 line ratios indicate electron densities closer to 10^{13} cm^{-3} at all epochs, but this high density appears to result from unresolved blending of λ97.88 by one or more lines. The λ142.20 line is very density sensitive, but it is never more than weakly detected at best. Using an electron density of 10^{12} cm^{-3}, we calculate

$$\mathrm{VEM} = 4\pi d^2 \frac{f}{T_{IS}} \frac{1}{\epsilon_{12}} \mathrm{cm}^{-3}, \quad (1)$$

where d is the distance to Capella (12.5 pc) and ϵ_{12} is the line emissivity. The volume emission measure provides a scaling of the individual line fluxes to produce an estimate of the amount of emitting plasma at the temperature of dominant formation for each line. This form of VEM assumes that all emitted photons are detected; if the corona is compact, the physical volume emission measure will be a factor of 2 larger because of the absorption of the downward-emitted photons by the photosphere.

The derived VEM values for λ128.73 and λ102.22 are naturally consistent since they were used to estimate the appropriate electron density. The VEM for the λ97.88 line is a factor of 2 higher, but this could be due to the aforementioned problem of a line blend. We find that the values for

TABLE 3

CORONAL EMISSION LINE FLUXES AND EMISSION MEASURES

Ion	λ (Å)	log T_e (K)	Date	f (10^{-13} ergs cm^{-2} s^{-1})	log VEM$_{(\text{for } N_e = 10^{12} \text{ cm}^{-3})}$ (10^{50} cm^{-3})
Fe XXI	1354.08	7.0	1995 Sep 9	1.07 ± 0.4	52.68
Fe XXI ($T_{IS} = 0.867$)	128.73	7.0	1992 Dec 10–13	2.2 ± 0.3	51.93
			1993 Dec 22–25	2.5 ± 0.3	51.99
			1994 Feb 15–16	4.8 ± 0.5	52.27
			1994 Feb 25–27	4.6 ± 0.4	52.25
			1995 Nov 30–Dec 4	3.7 ± 0.4	52.16
Fe XXI ($T_{IS} = 0.945$)	97.88	7.0	1992 Dec 10–13	1.2 ± 0.2	52.49
			1993 Dec 22–25	1.0 ± 0.2	52.41
			1994 Feb 15–16	1.0 ± 0.2	52.41
			1994 Feb 25–27	1.4 ± 0.2	52.55
			1995 Nov 30–Dec 4	1.1 ± 0.3	52.45
Fe XXI ($T_{IS} = 0.939$)	102.22	7.0	1992 Dec 10–13	0.9 ± 0.2	52.00
			1993 Dec 22–25	1.1 ± 0.2	52.09
			1994 Feb 15–16	1.5 ± 0.3	52.23
			1994 Feb 25–27	1.2 ± 0.2	52.13
			1995 Nov 30–Dec 4	1.2 ± 0.2	52.13
Fe XXI ($T_{IS} = 0.836$)	142.27	7.0	1992 Dec 10–13	0.77 ± 0.24	52.71:
Fe XIX ($T_{IS} = 0.929$)	108.37	6.9	1992 Dec 10–13	4.4 ± 0.3	52.35
			1993 Dec 22–25	3.5 ± 0.3	52.25
			1994 Feb 15–16	6.1 ± 0.4	52.49
			1994 Feb 25–27	6.8 ± 0.4	52.54
			1995 Nov 30–Dec 4	7.8 ± 0.4	52.60
Fe XVIII ($T_{IS} = 0.950$).....	93.92	6.8	1992 Dec 10–13	7.3 ± 0.4	52.56
			1993 Dec 22–25	5.3 ± 0.4	52.42
			1994 Feb 15–16	8.4 ± 0.6	52.62
			1994 Feb 25–27	8.4 ± 0.6	52.62
			1995 Nov 30–Dec 4	10.1 ± 0.6	52.70

the λ1354 line are even higher, with the λ1354 line a factor of 3.3 stronger than λ128.73. The Fe XIX and XVIII emission measures are also significantly larger, with values typically $\sim$0.5 dex higher than for Fe XXI λ128.73.

There are several possible explanations for the much larger VEM of Fe XXI λ1354 compared with the EUV Fe XXI lines: (1) the coronal Fe XXI emission is known to be variable, and the λ1354 line was observed when the high-temperature emission happened to be larger than during the *EUVE* observations; (2) the λ1354 line is formed preferentially at slightly lower temperatures than the other Fe XXI lines where the VEM is larger; (3) the fit to the C I/Fe XXI blend is contaminated by the presence of additional weak emission lines; or (4) the atomic data used are incorrect or incomplete. We have investigated the last option thoroughly and can see nothing to suggest that the atomic data used by Brickhouse et al. or by CHIANTI are inaccurate. In fact, the atomic data are relatively secure, and the collision strengths are probably good to 10% (e.g., Aggarwal 1991; Aggarwal et al. 1997). The possibility of additional blending with the λ1354 line is low given the absence of observed blending emission lines in *SOHO*/SUMER solar limb spectra (T. R. Ayres 1997, private communication). This leaves the first two possible explanations of which we think that variability is the most plausible because variations of up to a factor of 4 are present in the *EUVE* fluxes of ions hotter than Fe XIX obtained at different times (Brickhouse et al. 1997).

Dupree et al. (1993) have called attention to a peak (called a "bump") in the Capella emission measure distribution near log $T = 6.8$, which they argue is not an artifact of the analysis method. They speculate that the bump may be due to a magnetically active region or a shock interface between the stars where their winds collide. The roughly equal contribution of both stars to the Fe XXI λ1354 flux suggests another explanation. Approximately half of the Fe XXI emission is formed at or below log $T = 6.8$, and half above this temperature. If one of the Capella stars has a VEM(T) that increases to a maximum near log $T = 6.8$ with little plasma at higher temperatures, while the other star has a roughly constant VEM(T) extending to much higher temperatures, analysis of the combined spectrum could result in a continuous VEM(T) with a bump near log $T = 6.8$. Gehrels & Williams (1993) argue that the cooling coefficient for an optically thin coronal plasma has regions of thermal stability when the derivative of the cooling coefficient with temperature is positive. One of these stability regions is for log $T \leq 6.8$. Thus, a natural explanation for the bump in the VEM of the binary system would be that the heating rate in the corona of one star is insufficient to heat the plasma beyond log $T = 6.8$, while for the other star, the larger heating rate forces the plasma to higher temperatures in order to reach energy balance.

4. ANALYSIS OF THE He II λ1640 LINE

We observed the He II line twice: first at orbital phase 0.73 with the moderate-resolution G160M grating and then two orbits later at phase 0.78 with the GHRS Ech-A grating. These two profiles are compared in Figure 4 with the phase 0.26 profile obtained with the G160M grating on 1991 April 15 (Linsky et al. 1995). The phase 0.73 and 0.78 profiles are identical, except for the decrease in flux in the radial velocity interval -70 to 0 km s^{-1} at phase 0.78, corresponding to the radial velocity of the G8 star. The three He II spectra rely on three completely different flux calibrations: one for G160M observations made prior to the installation of the COSTAR corrective optics, one for post-COSTAR G160M data, and one for post-COSTAR Ech-A spectra. To ensure the accuracy of our flux calibrations, we compared the fluxes of the continuum surrounding the He II

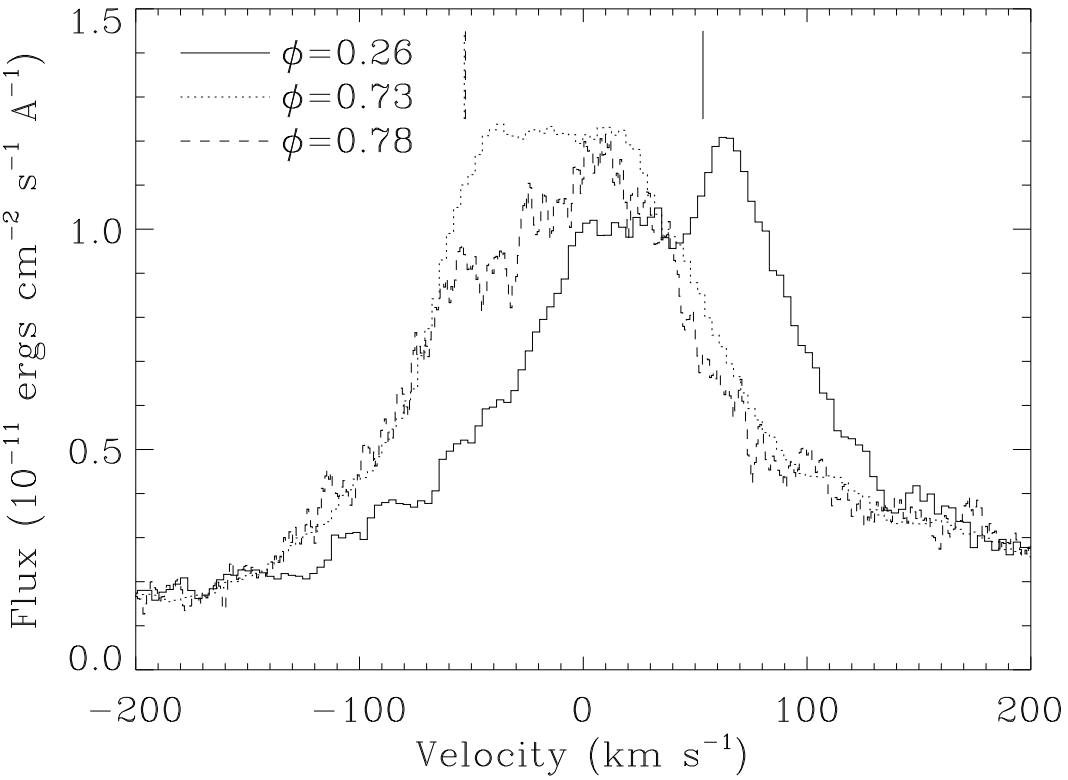

FIG. 4.—The He II λ1640 line profile of Capella (slightly smoothed) observed with the G160M grating at orbital phases 0.73 and 0.26, and with the Ech-A grating at phase 0.78. These spectra are plotted on a velocity scale in the photospheric rest frame of Capella's G1 star. The vertical lines mark the photospheric rest frame of the G8 star.

line for the three spectra. We found that the pre-COSTAR G160M fluxes agree perfectly with the post-COSTAR Ech-A spectrum, but we did have to increase the fluxes of the post-COSTAR G160M observation by 7% to be consistent with the other two spectra.

The Hα multiplet of He^+ centered near 1640 Å differs from the corresponding λ6563 Hα line of neutral hydrogen in that the $2p\ ^2P$ lower state of the transition lies 40.8 eV above the ground state for He^+ compared with only 10.2 eV for hydrogen. Two mechanisms have been proposed to explain the excitation of this line: (1) collisional excitation (CE) of the excited states of He^+ in the 1×10^5 K transition region plasma (e.g., Jordan 1975), and (2) radiative recombination (RR) and cascade, following photoionization of ground-state He^+ by EUV photons with $E > 45$ eV (e.g., Zirin 1975). Both excitation processes can be important at the same time. Wahlstrom & Carlsson (1994) have argued that RR is the dominant process for the Sun, while Athay (1988) has argued that CE also plays a major role in the Sun.

An empirical discriminant between these two mechanisms is that the CE model predicts a broad profile centered at a rest wavelength of 1640.438 Å (Feldman et al. 1975), whereas the RR model predicts a narrower profile, with two components of the He II multiplet dominating the emission, the strongest being the $2p\ ^2P_{3/2}$–$3d\ ^2D_{5/2}$ transition at 1640.474 Å. Based on the phase 0.26 observations, Linsky et al. (1995) suggested that the λ1640 line is formed mostly by CE in the transition region of the G1 star, while about 10% of the flux can be attributed to formation by the RR process in the chromosphere of the G8 star. Wood & Ayres (1995) found that the extensive set of *IUE* observations of Capella supported the conclusion that the CE mechanism dominates on the G1 star and the RR mechanism dominates on the G8 star, but they also demonstrated that the G8 star must contribute more flux to the He II line than suggested by the model of Linsky et al. (1995). The new observations show that the situation is even more complex than previously imagined.

At phases 0.73 and 0.78, the G8 star component should be located at -53 km s^{-1} (-0.29 Å) relative to the G1 star component. This is the only portion of the line profile where the phase 0.73 and 0.78 data differ substantially (see Fig. 4). This implies that the EUV radiation produced in the G8 star's corona, which is responsible for photoionizing He^+ and producing much of the λ1640 emission from the G8 star, is much weaker at the time of the phase 0.78 observation than at phase 0.73.

Since our three He II spectra sampled both orbital quadratures, we expected to separate accurately the G1 and G8 stars' contributions to the He II line. However, variability of the line flux and shape complicates this separation immensely. We began the analysis by trying to model the G1 and G8 star emission with single Gaussians. We fitted all three spectra simultaneously to constrain the fit as fully as possible. Although we allowed the flux of the G8 component (but not its width or velocity relative to the star) to vary among the three spectra, we could not find an acceptable fit to the data. Thus, we found it necessary to add a third Gaussian component to the analysis—a component with constant flux representing additional emission from the G8 star. Even with the addition of this component, we found that the only way we could obtain a reasonable fit to the He II lines at all three orbital phases was to allow the

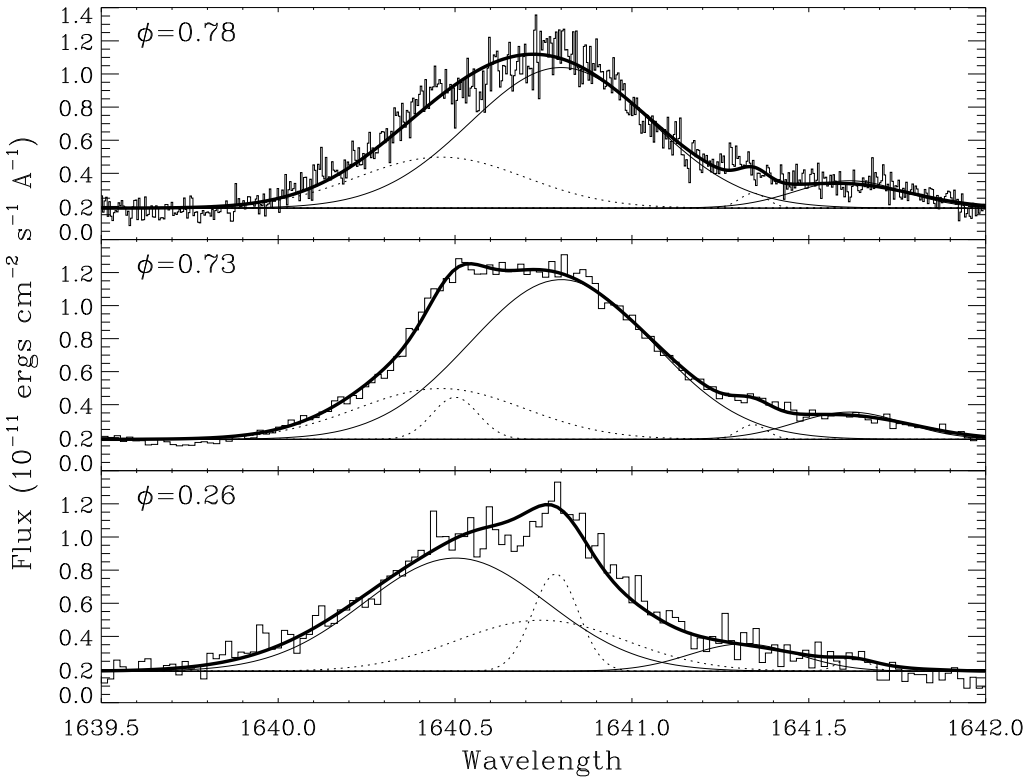

FIG. 5.—Observed profiles of the He II λ1640 line at three orbital phases with a complex multi-Gaussian fit to each line. The weaker O I λ1641.3 line is also visible in the far red wing of He II. The dotted lines represent emission components from the G8 star, while the thin solid lines are the G1 star's emission components (see text for a full description of these components). The thick solid lines are the sum of the components after convolution with the instrumental and rotational broadening profiles.

flux of the G1 star's Gaussian to vary among the three spectra, meaning that both Capella stars appear to have variable He II emission.

Figure 5 shows the final multi-Gaussian fit that resulted from this analysis, and Table 4 lists the parameters of this fit. In addition to the three He II components, we also had to include two components (one for each star) to account for the O I λ1641.3 line in the far red wing of He II. To minimize the number of free parameters in the fit, we forced the O I line widths and velocities to be identical to those measured for the O I] λ1358.5 line (see Table 2). When we initially performed this fit to the He II and O I line blend, the flux of the variable G8 star component ended up slightly negative for the $\phi = 0.78$ spectrum. Since we could think of no situation in which this line could be in absorption, we fixed the flux of this component to be exactly 0 at $\phi = 0.78$ and performed the fit again.

The final simultaneous fit to the He II + O I blend at all three orbital phases required 14 free parameters (see Table 4). Given that we allowed the fluxes of two components to vary from line to line, it is possible that other parameters, including line widths and velocities, also vary, but mini-

TABLE 4

MULTI-GAUSSIAN FIT PARAMETERS TO THE He II λ1640 LINE[a]

Orbital Phase	Ion	λ_{rest} (Å)	Star	λ_{meas} (Å)	v^b (km s^{-1})	f (10^{-13})	FWHM (km s^{-1})
$\phi = 0.26$.....	He II	1640.428[c]	G1	1640.502	11 ± 1	44.2 ± 1.5	111 ± 2
			G8	1640.743	2 ± 2	18.3 ± 1.4	102 ± 3
			G8	1640.784	10 ± 1	9.6 ± 1.3	28 ± 3
	O I	1641.305	G1	1641.316	(0)	6.4 ± 0.2	(66)
			G8	1641.626	(3)	0.9 ± 0.1	(17)
$\phi = 0.73$.....	He II	1640.428[c]	G1	1640.801	11 ± 1	62.6 ± 2.5	111 ± 2
			G8	1640.459	2 ± 2	18.3 ± 1.4	102 ± 3
			G8	1640.500	10 ± 1	4.2 ± 0.7	28 ± 3
	O I	1641.305	G1	1641.615	(0)	6.4 ± 0.2	(66)
			G8	1641.342	(3)	0.9 ± 0.1	(17)
$\phi = 0.78$.....	He II	1640.428[c]	G1	1640.800	11 ± 1	54.9 ± 2.4	111 ± 2
			G8	1640.460	2 ± 2	18.3 ± 1.4	102 ± 3
			G8	1640.501	10 ± 1	(0.0)	28 ± 3
	O I	1641.305	G1	1641.614	(0)	6.4 ± 0.2	(66)
			G8	1641.343	(3)	0.9 ± 0.1	(17)

[a] Values in parentheses are assumed rather than derived.
[b] The line velocity relative to the star responsible for the emission.
[c] Centroid laboratory wavelength for the radiative recombination model.

mizing the number of free parameters as we have done has the virtue of simplicity, and it assures us a unique fit. One could reduce the complexity of the fit still further by not allowing any of the existing components to vary and then adding a variable absorption component fixed at 1640.6 Å in all three spectra. Circumstellar He II absorption would appear to be the only interpretation for such a component, but this is very unlikely. Since the $n = 2$ level of He II lies 40.8 eV above the ground state and is rapidly depopulated by the resonance transition (304 Å), there should be only a very small population of the $n = 2$ level and thus no detectable λ1640 absorption line.

4.1. *Which Mechanism is Most Important in Producing the* He II λ1640 *Line for Each Star?*

Our preferred model, shown in Figure 5, includes only emission components that follow the stellar velocities as they change with orbital phase. With a reduced χ^2 value of $\chi^2_\nu = 1.503$, the quality of the fit is respectable but not perfect. Although this model is probably the simplest that could fit the data well, it is still very complex and difficult to interpret. We do not believe it would be wise to assign any meaning to the broad and narrow components representing the He II emission from the G8 star, but we do believe that the sum of the two components is a much better estimate for the actual He II profile and flux of the G8 star than the extremely narrow G8 component proposed by Linsky et al. (1995). Their result implies a very low He II flux from the G8 star, which is inconsistent with the line centroid variations with orbital phase obtained by Wood & Ayres (1995) from their analysis of an extensive set of *IUE* observations. The G8 star's flux contribution in our model, which varies between 25% and 40% (see Table 4), is large enough to be consistent with the Wood & Ayres (1995) data. Furthermore, the larger flux contribution from the G8 star in our model decreases the empirical velocity of the G1 star's He II emission from 32 km s^{-1} (Linsky et al. 1995) to 11 km s^{-1}, which is more consistent with average transition region line redshifts observed for the G1 star.

Our model shows that the G1 star dominates the He II λ1640 flux, but our analysis of the Fe XXI λ1354 line and the work of Ayres et al. (1983) both conclude that the G1 and G8 stars have roughly equal coronal fluxes. Thus, the RR mechanism should be a more important contributor to the G8 star's λ1640 flux than it is for the G1 star, as previously suggested by Linsky et al. (1995) on the basis of the narrowness of the G8 star's He II emission. However, our detection of significantly variable λ1640 emission from the G1 star suggests that the RR mechanism must be present to some extent on this star as well because Capella's transition region line emission is remarkably constant with time (see, e.g., Wood & Ayres 1995), making it very hard for the CE model, in which the electron collisions occur primarily at transition region temperatures, to explain the He II variability. We therefore conclude that the He II variations detected for both stars are probably produced by coronal variations. Note that the total He II flux is largest at $\phi = 0.73$ when the Fe XXI λ1354 line was observed, and we have already argued that the Fe XXI flux was larger than normal at that time (see § 3.3), consistent with our He II interpretation.

Using *EUVE* spectra of the Capella system obtained in 1992 December, Dupree et al. (1993) estimated that the He II λ1640 line flux produced by the RR process alone should be 16×10^{-13} ergs cm^{-2} s^{-1}. If the *EUVE* flux from each star scales as the Fe XXI λ1354 flux, then the λ1640 emission produced by the RR mechanism should be about 8×10^{-13} ergs cm^{-2} s^{-1} for both the G1 star and G8 star. The *EUVE* fluxes listed in Table 3 suggest that the observation analyzed by Dupree et al. (1993) had lower fluxes than average, and that Capella's EUV fluxes can be a factor of 2 higher. Also, we have argued that the *EUVE* fluxes were high at phase 0.73 when one of the He II observations were obtained. We therefore estimate that the rate of He II λ1640 excitation by the RR process at the times of the He II observations corresponds to an EUV flux of 16×10^{-13} ergs cm^{-2} s^{-1} for each star. Comparing this predicted flux with the He II fluxes assigned to each of the two stars listed in Table 4, we find that these *EUVE* results are consistent with our model in which the He II emission from the G8 star [observed to lie in the range $(18.3–27.9) \times 10^{-13}$] is excited primarily by the RR mechanism, whereas the emission from the G1 star [observed to lie in the range $(44.2–62.6) \times 10^{-13}$] is excited primarily by the CE mechanism. The implied variability in the G1 star's He II emission due to the RR component (roughly 8×10^{-13} ergs cm^{-2} s^{-1}) is about factor of 2 smaller than the G1 star variability suggested by our He II model (see Table 4). This indicates that the CE component of the G1 star's He II emission may also be variable, but we have no independent data that could confirm this conclusion.

5. ARE Fe XXI AND He II LINES PROVIDING A SELF-CONSISTENT PICTURE OF CAPELLA'S CORONA?

We conclude by asking whether our analysis of the high-resolution ultraviolet Fe XXI and He II lines is providing a self-consistent, credible picture of Capella's corona. While high-resolution spectroscopy provides new and important information on the volume emission measures, flow velocities, and turbulence in the coronae surrounding each star, this technique has limitations. One is that the Fe XXI line only samples the amount of 10^7 K plasma, whereas the He II line is formed in part by the RR processes that are driven by all coronal radiation at wavelengths less than 228 Å, consisting of lines and continuum formed over a wide range of temperatures. Thus, the shape of the volume emission measure distribution plays a critical role, but the shape must be inferred from other data sets. Our result that the 10^7 K plasma is not flowing, and therefore confined by magnetic fields, only refers to the hot plasma in the coronae of these stars. Our spectra provide no information on the kinematics of the cooler coronal plasmas that we know exist on the basis of *ROSAT*, *ASCA*, and *EUVE* data. In particular, we have no information on the coronal winds of these stars. These questions and others await high-resolution X-ray or EUV spectroscopy and/or more sensitive UV spectroscopy that could study coronal lines formed at lower temperatures.

This work is supported by Space Telescope Science Institute grant GO-05886.01.94A and NASA grants NAG 5-3226 and NAG 5-2259 to the University of Colorado. This work is based on observations with the NASA/ESA *Hubble Space Telescope*, obtained at the Space Telescope Science Institute, which is operated by the Association of Universities for Research in Astronomy, Inc., under NASA contract NAS5-26555. We thank Marc Gagné for advice in using his code to extract the *EUVE* line fluxes, and Nancy Brickhouse for helpful comments on the manuscript.

REFERENCES

Aggarwal, K. M. 1991, ApJS, 77, 677
Aggarwal, K. M., Hibbert, A., Keenan, F. P., & Norrington, P. H. 1997, ApJS, 108, 575
Arnaud, M., & Raymond, J. 1992, ApJ, 398, 394
Athay, R. G. 1988, ApJ, 329, 482
Ayres, T. R. 1984, ApJ, 284, 784
———. 1988, ApJ, 331, 467
Ayres, T. R., Schiffer, F. H., III, & Linsky, J. L. 1983, ApJ, 272, 223
Brandt, J. C., et al. 1994, PASP, 106, 890
Brickhouse, N. S., Dupree, A. K., Edgar, R. J., Drake, S. A., White, N. E., Liedahl, D. A., & Singh, K. P. 1997, BAAS, 29, 808
Brickhouse, N. S., Raymond, J. C., & Smith, B. W. 1995, ApJS, 97, 551
Carpenter, K. C., Robinson, R. D., Wahlgren, G. M., Ake, T. B., Ebbets, D. C., Linsky, J. L., Brown, A., & Walter, F. M. 1991, ApJ, 377, L45
Dere, K. P., Monsignori-Fossi, B. C., Landini, E., Mason, H. E., & Young, P. R. 1996, BAAS, 28, 961
Dupree, A. K., Brickhouse, N. S., Doschek, G. A., Green, J. C., & Raymond, J. C. 1993, ApJ, 418, L41
Feldman, U., Doschek, G. A., Van Hoosier, M. E., & Tousey, R. 1975, ApJ, 199, L67
Gagné, M., Valenti, J. A., Linsky, J. L., Brown, A., & Tagliaferri, G. 1997, in preparation
Gehrels, N., & Williams, E. D. 1993, ApJ, 418, L25
Gilliland, R. L. 1994, GHRS Instrum. Sci. Rep. 063 (Baltimore: STScI)
Heap, S. R., et al. 1995, PASP, 107, 871
Jordan, C. 1975, MNRAS, 170, 429
Lenz, D. D., & Ayres, T. R. 1992, PASP, 104, 1104
Linsky, J. L., et al. 1993, ApJ, 402, 694
Linsky, J. L., Wood, B. E., Judge, P., Brown, A., Andrulis, C., & Ayres, T. R. 1995, ApJ, 442, 381
Maran, S. P., et al. 1994, ApJ, 421, 800
Robinson, R. D., Airapetian, V. S., Maran, S. P., & Carpenter, K. G. 1996, ApJ, 469, 872
Sandlin, G. D., Bartoe, J.-D. F., Brueckner, G. E., Tousey, R., & Van Hoosier, M. 1986, ApJS, 61, 601
Sandlin, G. D., Brueckner, G. E., & Tousey, R. 1977, ApJ, 214, 898
Soderblom, D. R., Hulbert, S. J., Leitherer, C., & Sherbert, L. E. 1994, *HST* Goddard High-Resolution Spectrograph Instrument Handbook, Version 5.0 (Baltimore: STScI)
Strassmeier, K. G., & Fekel, F. C. 1990, A&A, 230, 389
Wahlstrom, C., & Carlsson, M. 1994, ApJ, 433, 417
Wood, B. E., & Ayres, T. R. 1995, ApJ, 443, 329
Wood, B. E., Harper, G. M., Linsky, J. L., & Dempsey, R. C. 1996, ApJ, 458, 761
Wood, B. E., & Linsky, J. L. 1997, ApJ, 474, L39
Zirin, H. 1975, ApJ, 199, L63